Linear stability of a thin fluid film interacting with its surrounding bulk fluid

By S. Mirjalili AND W. H. R. Chan

1. Motivation and objectives

The study of thin fluid films is of practical importance for various geophysical, biophysical, and engineering flows (Oron *et al.* 1997; Craster & Matar 2009; Kirkinis & Davis 2015; Zhao & Patankar 2020, and references therein). These films are often stabilized by surface tension. This work considers films that are sufficiently thin for the destabilizing effect of intermolecular van der Waals forces to also be important. The spontaneous rupture of thin liquid films due to van der Waals forces and electric double-layer repulsion was investigated by various researchers (Vrij 1966; Sheludko 1967; Vrij & Overbeek 1968; Ivanov *et al.* 1970). Their linear stability was specifically analyzed by Ruckenstein & Jain (1974) and González *et al.* (2016). The time evolution of these films was subsequently considered in the context of nonlinear stability (Williams & Davis 1982; Prévost & Gallez 1986; Sharma & Ruckenstein 1986*a*,*b*; Yiantsios & Higgins 1991; Erneux & Davis 1993), and then from the perspective of self-similar rupture (e.g., Ida & Miksis 1996; Zhang & Lister 1999; Vaynblat *et al.* 2001; Moreno-Boza *et al.* 2020*a*,*b*). In all these studies, the effect of the flow inside the surrounding bulk fluid was assumed to be negligible. This assumption was based on the relatively small viscosity, density, and inertia of the surrounding bulk fluid—typically air—compared with that of the fluid inside the film, which is typically some liquid.

In general, the effect of the surrounding bulk cannot be neglected for all film–bulk fluid pairings. For instance, Kaur & Leal (2009) extended the work of Baldessari *et al.* (2007) to consider the problem of coalescence of small viscous drops in emulsions, where the flow of the surrounding bulk fluid can no longer be neglected. They analyzed viscous contributions to the pressure gradients in thin liquid films due to flows in the two coalescing drops entrapping the film, as well as the consequences of the mobility of the sandwiched phase interfaces. This work aims to generalize the stability analysis of thin fluid films to various film–bulk fluid pairs in the limits of potential flow and Stokes flow for the bulk flow surrounding the film. Dispersion relations are provided for each limit, in addition to a regime diagram that specifies when each limit holds.

The ensuing theoretical analysis in Sections 2–4 is particularly relevant to situations in which the bulk flow plays a major role in the instability mechanism. In addition to coalescence in emulsions and its implications on emulsion stability in biochemical, materials, and chemical engineering applications, such situations arise in the Mesler entrainment of microbubbles and the generation of thin gas films in oceans and molten salt reactors with an eye to ionic-liquid-based carbon capture processes; the collision and spreading of superfluid drops with an eye to precision manufacturing of nanoparticles and nanowires; and the formation and stability of antibubbles and porous liquids, with specific fluid pairings discussed in Section 5.

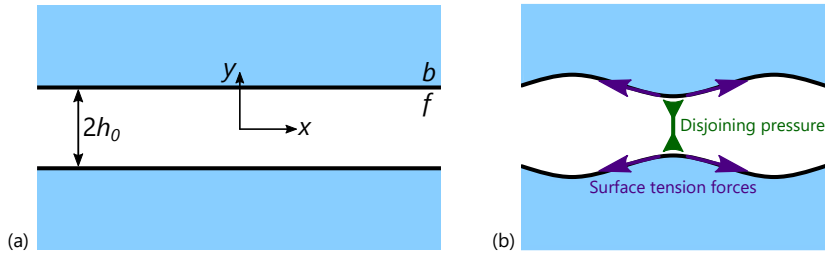

FIGURE 1. (a) Schematic of an unperturbed thin film surrounded by bulk fluid. (b) Schematic of interplay between disjoining pressure and surface-tension forces in a perturbed thin film surrounded by bulk fluid for the analysis of Section 3.

2. Problem setup

For simplicity, this work focuses on the stability of a two-dimensional thin fluid film of mean thickness $2h_0$ sandwiched by initially stationary fluids of another phase extending semi-infinitely in opposite directions normal to the unperturbed interfaces. A schematic of this configuration is shown in Figure 1(a). Since the base state is static, the film is nondraining and there is no mean flow in either of the phases. This assumption is appropriate in the limit where the time scale of the instability is much shorter than the time scales of other physical effects; i.e., when a quasi-static approximation is valid. While the dispersion relations obtained from a quasi-one-dimensional analysis may not be immediately applicable when the film has a quasi-two-dimensional and/or complex geometry, the findings of this work can be useful in the limit where the length scales governing the unstable modes are much smaller than the other pertinent length scales of the system. Gravitational forces, surface-tension gradients and electrokinetic effects are neglected in this analysis. As noted in Section 1, the problem is examined in the two limits of potential flow and Stokes flow in the bulk in Sections 3 and 4, respectively. In both cases, lubrication flow is assumed in the thin film. By analyzing the time and length scales of relevance, we clarify the conditions for the validity of these limits.

3. Bulk potential flow

3.1. *Governing equations*

In this section, it is assumed that the flows within the bulk are potential while the lubrication approximation holds for the film. Consider a coordinate system in which the film is aligned with the x-coordinate, while the y-coordinate is normal to the undisturbed film interfaces and $y = 0$ is at the centerline of the film, as depicted in Figure 1. Only one of the bulk sections is considered due to symmetry about the $y = 0$ line. In dimensional form, the normal stress balance at the interface yields

$$P_f = P_b|_{y=h} + \frac{A_H}{(2h)^3} - \sigma \frac{\partial^2 h/\partial x^2}{\left[1 + (\partial h/\partial x)^2\right]^{3/2}}, \tag{3.1}$$

where P denotes the hydrodynamic pressure, $2h$ is the thickness of the film, and the unretarded approximation for the van der Waals force is used to model the disjoining pressure contribution. Also, A_H is the dimensional Hamaker constant for the system, σ is the surface-tension coefficient, and the subscripts f and b denote quantities in the film and bulk, respectively. After substituting for P_f from Eq. (3.1), lubrication theory for

the thin film yields

$$\frac{\partial h}{\partial t} = \frac{1}{3\mu_f}\frac{\partial}{\partial x}\left[h^3\left(\left.\frac{\partial P_b}{\partial x}\right|_{y=h} + \frac{\partial}{\partial x}\frac{A_H}{8h^3} - \sigma\frac{\partial^3 h}{\partial x^3}\right)\right] - \frac{\partial(h u_b|_{y=h})}{\partial x}, \tag{3.2}$$

where μ_f is the dynamic viscosity of the film. Note that the velocity field in the bulk is denoted $\vec{u}_b = (u_b, v_b)$. Potential flow theory for the flow in the bulk yields

$$\frac{D\vec{u}_b}{Dt} = -\frac{1}{\rho_b}\nabla P_b, \tag{3.3}$$

where D/Dt denotes the material derivative and ρ_b is the bulk density, while the kinematic boundary condition at the interface reads

$$\frac{\partial h}{\partial t} = v_b|_{y=h} - u_b|_{y=h}\frac{\partial h}{\partial x}. \tag{3.4}$$

To derive the linearized form of the equations, perturbations—denoted prime ($'$)—are introduced about the base state (denoted subscript 0). For instance, $h = h_0 + h'$. This results in

$$\frac{\partial h'}{\partial t} = -\frac{\partial(h_0 u_b'|_{y=h_0})}{\partial x} + \frac{1}{3\mu_f}\left(h_0^3\left.\frac{\partial^2 P_b'}{\partial x^2}\right|_{y=h_0} - \frac{3A_H}{8h_0}\frac{\partial^2 h'}{\partial x^2} - \sigma h_0^3\frac{\partial^4 h'}{\partial x^4}\right), \tag{3.5}$$

$$\frac{\partial \vec{u}_b'}{\partial t} = -\frac{1}{\rho_b}\nabla P_b', \tag{3.6}$$

$$\frac{\partial h'}{\partial t} = v_b'|_{y=h_0}, \tag{3.7}$$

as the linearized versions of Eqs. (3.2)–(3.4).

3.2. *Dispersion relation and nondimensionalization*

Continuity in the bulk phase, coupled to Eqs. (3.3) and (3.6), implies that both the bulk pressure and its perturbation should satisfy the Laplace equation. Normal-mode analysis for temporal stability then admits solutions in the form of

$$\begin{bmatrix} P_b' \\ \vec{u}_b' \\ h' \end{bmatrix} = \begin{bmatrix} \hat{P}_b e^{-ky} \\ \hat{\vec{u}}_b e^{-ky} \\ \hat{h} \end{bmatrix} e^{\omega t + \mathrm{i}kx}. \tag{3.8}$$

After plugging Eq. (3.8) into Eqs. (3.5)–(3.7), the dispersion relation for temporal stability can be obtained in dimensional form as

$$\left(\rho_b k h_0^3\right)\omega^2 + \left(3\mu_f\right)\left(1 + h_0 k\right)\omega + \sigma h_0^3 k^4 - \frac{3A_H}{8h_0}k^2 = 0. \tag{3.9}$$

Previous studies of the stability of thin liquid films (Vrij 1966; Vrij & Overbeek 1968; Ruckenstein & Jain 1974) and experimental observations of gas films (Couder *et al.* 2005; Dorbolo *et al.* 2005; Thoroddsen *et al.* 2012) have shown that for sufficiently large wavelengths, perturbations due to the attractive disjoining pressure cannot be stabilized by surface-tension forces. A schematic of the interplay between these two forces is shown in Figure 1(b). By balancing these two forces, the critical wavelength is found to scale as $\lambda_{cr} \sim h_0^2\sqrt{\sigma/A_H}$. Using this length scale, the nondimensional wave number is defined as $\tilde{k} = kh_0^2\sqrt{\sigma/A_H}$. Note that this implies that a lower surface-tension coefficient reduces

the length scale at which this instability becomes active. For a fixed pair of working fluids, the only physical parameter for the problem is the film thickness, which is alternatively specified using the Laplace number

$$La = \frac{1}{Oh^2} = \frac{\rho_b h_0 \sigma}{\mu_f^2}. \tag{3.10}$$

The strength of the intermolecular van der Waals forces is then parameterized by

$$\tilde{A}_H = A_H \frac{\rho_b^2 \sigma}{\mu_f^4}. \tag{3.11}$$

Assuming that the axial scale of the problem scales with the critical wavelength, and also that attractive intermolecular forces are the driver of instabilities, Eq. (3.5) can then be used to find the relevant time scale of the instability, which would scale as $\tau \sim \sigma h_0^5 \mu_f / A_H^2$. If this time scale is used to nondimensionalize the growth rate, $\tilde{\omega} = \omega(\sigma h_0^5 \mu_f)/(A_H^2)$, then the dispersion relation in Eq. (3.9) can be written in nondimensional form as

$$\tilde{A}_H^{5/2} La^{-4} \tilde{k} \tilde{\omega}^2 + 3(1 + \tilde{A}_H^{1/2} La^{-1} \tilde{k}) \tilde{\omega} + \tilde{k}^4 - 3\tilde{k}^2/8 = 0, \tag{3.12}$$

which is a quadratic equation in terms of the nondimensional growth rate, $\tilde{\omega}$. It is worth noting that the unstable solutions to this dispersion relation are purely real.

3.3. *Regime of instability and notable limits*

In Figure 2, the nondimensional growth rate, which is purely real for unstable modes, is plotted as a function of the nondimensional wave number for various La with $\tilde{A}_H = 3.354 \times 10^4$. As a practical example, consider an air film surrounded by water. If the Hamaker constant is taken to be $A_H = 5 \times 10^{-20}$ kg m^2 s^{-2}, then the air film thicknesses shown in Figure 2 would be $h_0 = 455.0$ nm, 45.5 nm, 4.55 nm, and 0.455 nm, corresponding to $La = 10^5, 10^4, 10^3$, and 10^2, respectively. Due to the large viscosity of water, a Stokes flow rather than a potential flow actually develops in the water bulk for most of the larger film thicknesses considered, as clarified in Section 3.4. This film–bulk fluid pair is thus used here only as an example for illustration purposes, and more relevant fluid pairs where the bulk can be treated with potential flow theory for a larger range of film thicknesses are discussed in Section 5.

A few observations can be made from Eq. (3.12) and Figure 2. First, the system is unstable for $\tilde{k} < \sqrt{3/8}$, corresponding to dimensional wavelengths larger than $\lambda_{cr} = 10.26\sqrt{\sigma/A_H} h_0^2$. This is in general agreement with the expected wavelength scaling from scaling analysis. Second, one can see from Figure 2 that while La—and thus the film thickness—spans three orders of magnitude, $\tilde{\omega}$ varies within one order of magnitude. This demonstrates agreement with the earlier scaling analysis, $\tilde{\omega} \sim A_H^2/(\sigma h_0^5 \mu_f)$, meaning that attractive van der Waals forces reduce the time scale of instability (destabilize the system), while larger surface tension, film fluid viscosity, and film thickness increase the time scale of instability (stabilize the system). Third, observe that the nondimensional growth rates for the three thickest films in Figure 2 almost collapse. This is because $\tilde{A}_H^{5/8} \ll La$ for these films, as a result of which the first term in Eq. (3.12) can be ignored. This term corresponds to the contribution from the pressure buildup due to potential flow in the bulk. Additionally, because $\tilde{A}_H^{1/2} \ll La$ for these three films, the second term in the parentheses in Eq. (3.12), corresponding to the contribution from the movement of the interface in the x-direction, i.e., the pressure induced by the surface velocity perturbation, can also be ignored. In Section 3.4, we show that this condition

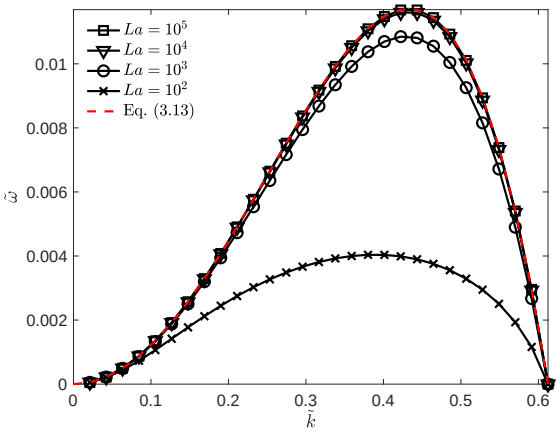

FIGURE 2. Dispersion relation, Eq. (3.12), for various values of La with $\tilde{A}_H = 3.354 \times 10^4$.

is required for the thin film assumption to be valid. Note that these two conditions on the dimensionless parameters are not valid for $La = 10^2$ in Figure 2. If both of these conditions hold, then the flow in the bulk does not significantly affect the dynamics of the instability, and the dispersion relation in Eq. (3.12) reduces to

$$\tilde{\omega} \approx \frac{1}{3}\left(\frac{3}{8}\tilde{k}^2 - \tilde{k}^4\right), \tag{3.13}$$

which matches the dispersion relation for the stability of a free thin liquid film surrounded by a low-viscosity and low-density fluid such as air (Ruckenstein & Jain 1974; Kirkinis & Davis 2015). The only physical constants (material properties) governing the instability in this case are the film viscosity, the surface tension, and the Hamaker constant. The dispersion relationship given by Eq. (3.13) is shown by the dashed line in Figure 2. It is clear that the three thickest films—and other films thicker than these films—have a dispersion relation that is very close to that in Eq. (3.13).

3.4. *Conditions for validity*

The validity of the analysis in Sections 3.2 and 3.3 is contingent on the assumptions of lubrication flow in the film and potential flow within the bulk. For lubrication flow to hold, we require the thin film approximation to hold, i.e., $h_0 \ll \lambda_{cr}$, which is equivalent to $\tilde{A}_H^{1/2} \ll La$. Note that $Re_{u'} \ll 1$ is automatically satisfied for the flow in the film as the flow magnitude scales linearly with the perturbation in the film thickness, h'. Note also that while a lower surface-tension coefficient increases the growth rate and destabilizes the system under this analysis, it also decreases λ_{cr} and thus the likelihood that the thin film approximation holds for a given film thickness h_0. The assumption of potential flow in the bulk depends on the viscosity of the bulk fluid. This adds one nondimensional parameter to La and $\tilde{A}_H$, given by the viscosity ratio, $\tilde{\mu} = \mu_f/\mu_b$. Two conditions must be met for potential flow to be valid in the bulk fluid sections. First, the shear from the thin film generates a boundary layer in the bulk. The perturbation in the surface velocity due to this effect can be neglected for durations on the order of or less than the characteristic time scale of the instability if $La \ll \tilde{A}_H^{2/3}\tilde{\mu}^{-1/3}$. Second, the time scale for the growth of the instability should be much smaller than the vorticity-diffusion time

scale required for the diffusion layer to reach a thickness of λ_{cr}, which is the characteristic length scale for the bulk potential flow along the interface-normal direction. This results in the condition $La \ll \tilde{A}_H\tilde{\mu}$. In short, the analysis in Sections 3.2 and 3.3 is valid if

$$\tilde{A}_H^{1/2} \ll La \ll \tilde{A}_H\tilde{\mu}, \tag{3.14}$$

$$La \ll \tilde{A}_H^{2/3}\tilde{\mu}^{-1/3}. \tag{3.15}$$

While the La range specified by Eqs. (3.14) and (3.15) yields a range of film thicknesses for which the analysis above is valid, it is clear that such films do not exist for some film–bulk fluid pairings. Revisiting Figure 2, for example, this condition only holds for $2 \times 10^2 \ll La \ll 7 \times 10^2$, or approximately $0.8\,\text{nm} \ll h_0 \ll 3\,\text{nm}$, for an air film surrounded by water. Evidently, this range of validity for h_0 is limited. More generally, $\tilde{A}_H^{-1/2} \ll \tilde{\mu} \ll \tilde{A}_H^{1/2}$ is a prerequisite for the existence of a range of film thicknesses in which potential flow in the bulk and lubrication theory in the film can be assumed. Note that this in turn requires $\tilde{A}_H \gg 1$. In Section 5, fluid pairings for which Eqs. (3.14) and (3.15) can hold for a range of viable film thicknesses, as well as pairings for which no such range exists, are examined.

4. Bulk Stokes flow

4.1. *Governing equations*

Consider now the Stokes-flow limit for the bulk, in which viscous effects dominate and inertial effects can be neglected. Instead of Eq. (3.3), the flow inside the bulk is a Stokes flow, satisfying

$$\frac{\partial \vec{u_b}}{\partial t} = -\frac{1}{\rho_b}\nabla P_b + \frac{\mu_b}{\rho_b}\nabla^2\vec{u_b}. \tag{4.1}$$

Again, only the bulk section with $y > 0$ is considered due to symmetry. Using the Green's function for Stokes flow, the velocity field and pressure within the bulk—including on the interface—can be evaluated from the shear stress exerted by the fluid film at $y = h$. This shear stress is given by $\mu_f(\partial u_f/\partial y) = h(\partial P_f/\partial x)$. The bulk fluid pressure on the interface is then given by

$$P_b|_{y=h} = \frac{1}{2\pi}\int_{-\infty}^{\infty} h(x_0)\frac{\partial P_f(x_0)}{\partial x_0}\frac{1}{x - x_0}\,\mathrm{d}x_0. \tag{4.2}$$

Similarly, the Green's function for Stokes flow can also be used to find the x-velocity of the bulk fluid on the interface,

$$u_b|_{y=h} = \frac{1}{4\pi\mu_b}\int_{-\infty}^{\infty} h(x_0)\frac{\partial P_f(x_0)}{\partial x_0}(-\ln|x - x_0| + 1)\,\mathrm{d}x_0. \tag{4.3}$$

The additional equations that govern the system are the balance of normal stresses on the interface, Eq. (3.1), and lubrication theory in the film, Eq. (3.2). If we use prime (') to denote the perturbations about the base state, then the linearized equations governing the problem are given by

$$P_b'|_{y=h_0} = \frac{h_0}{2\pi}\int_{-\infty}^{\infty}\frac{1}{x - x_0}\left(\left.\frac{\partial P_b'(x_0)}{\partial x_0}\right|_{y=h_0} - \frac{3A_H}{8h_0^4}\frac{\partial h'(x_0)}{\partial x_0} - \sigma\frac{\partial^3 h'(x_0)}{\partial x_0^3}\right)\mathrm{d}x_0, \tag{4.4}$$

$$u_b'|_{y=h_0} = \frac{h_0}{4\pi\mu_b}\int_{-\infty}^{\infty}(-\ln|x-x_0|+1)\times \left(\left.\frac{\partial P_b'(x_0)}{\partial x_0}\right|_{y=h_0} - \frac{3A_H}{8h_0^4}\frac{\partial h'(x_0)}{\partial x_0} - \sigma\frac{\partial^3 h'(x_0)}{\partial x_0^3}\right)\mathrm{d}x_0, \quad (4.5)$$

and Eq. (3.5). A similar set of equations was solved by Baldessari *et al.* (2007) and Kaur & Leal (2009) to determine the linear stability of a draining film between two drops in emulsions, with the main differences being that they assume uniform pressure within the bulk sections, as well as zero surface velocity perturbations. Note that most of the results of Baldessari *et al.* (2007) are in the large-$\tilde{\mu}$ limit.

4.2. *Dispersion relation and nondimensionalization*

To proceed, the normal-mode assumption is made, namely,

$$\begin{bmatrix} P_b'|_{y=h_0} \\ u_b'|_{y=h_0} \\ h' \end{bmatrix} = \begin{bmatrix} \hat{P}_{b,y=h_0} \\ \hat{u}_{b,y=h_0} \\ \hat{h} \end{bmatrix} e^{\omega t + \mathrm{i}kx}. \quad (4.6)$$

By plugging Eq. (4.6) into the integro-differential system of equations given by Eqs. (4.4), (4.5), and (3.5), the dispersion relation can be obtained in dimensional form as

$$\omega = \left(\frac{2kh_0^2}{3\mu_f}\right)\left[\frac{3\mu_f/(4\mu_b) - kh_0}{2 - kh_0}\right]\left(\sigma k^2 - \frac{3A_H}{8h_0^4}\right). \quad (4.7)$$

We utilize the same nondimensionalization as in Section 3.2 here, and include the viscosity ratio $\tilde{\mu} = \mu_f/\mu_b$ also introduced earlier in Section 3.4. The nondimensional dispersion relation for Stokes flow in the bulk is then given by

$$\tilde{\omega} = \frac{1}{3}\left(\frac{3}{8}\tilde{k} - \tilde{k}^3\right)\left[\frac{\tilde{k} - (3/4)\tilde{\mu}La\tilde{A}_H^{-1/2}}{1 - (1/2)La^{-1}\tilde{A}_H^{1/2}\tilde{k}}\right]. \quad (4.8)$$

4.3. *Regime of instability and notable limits*

Similar to Section 3.3, we utilize the physical parameters related to an air film surrounded by bulk sections of water to demonstrate some examples of the growth rate with respect to the wave number. For any pair of working fluids, two different scenarios can be observed depending on the magnitude of La (or the film thickness).

The first scenario that is observed for thinner films, $La < \sqrt{(2/3)}\tilde{A}_H^{1/2}\tilde{\mu}^{-1}$, is quite similar to the dispersion curves from potential flow theory (Section 3). Three examples of this scenario can be observed in Figure 3, where the nondimensional growth rate is plotted against nondimensional wave numbers for $La = 10^3, 5\times10^2$, and 10^2, corresponding to film thicknesses of 4.55 nm, 2.27 nm, and 0.455 nm, respectively, for $\tilde{A}_H = 3.354\times10^4$ and $\tilde{\mu} = 0.020$. Note again that these cases are only used for illustration purposes, as we show in Section 4.4 that the Stokes-flow analysis is only valid for these values of $\tilde{A}_H$ and $\tilde{\mu}$ when $La \gg 4\times10^3$. The unstable wave numbers are $(3/4)\tilde{\mu}La\tilde{A}_H^{-1/2} < \tilde{k} < \sqrt{3/8}$, corresponding to dimensional wavelengths in the range of $10.26\sqrt{\sigma/A_H}h_0^2 < \lambda < 8.378h_0(\mu_b/\mu_f)$. The upper bound for unstable wave numbers matches the potential flow theory. Moreover, the growth rate is also appropriately scaled by $A_H^2/(\sigma h_0^5\mu_f)$ since an order-of-magnitude variation in La changes the growth rate by less than an order of magnitude. The dispersion relation obtained from neglecting the effect of the bulk fluid, Eq. (3.13), is also plotted in Figure 3. We observe that while the growth-rate scaling

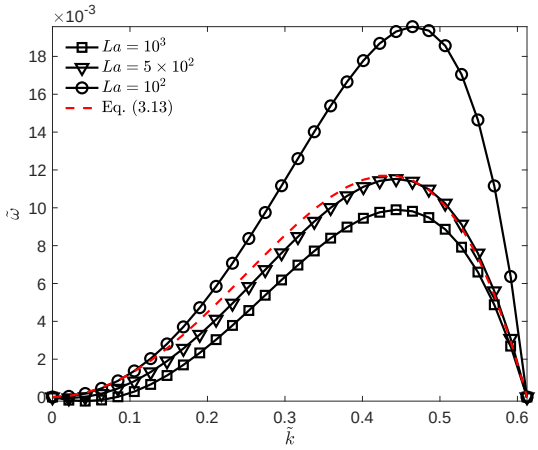

FIGURE 3. Dispersion relation, Eq. (4.8), for multiple values of La with $\tilde{A}_H = 3.354 \times 10^4$ and $\tilde{\mu} = 0.020$.

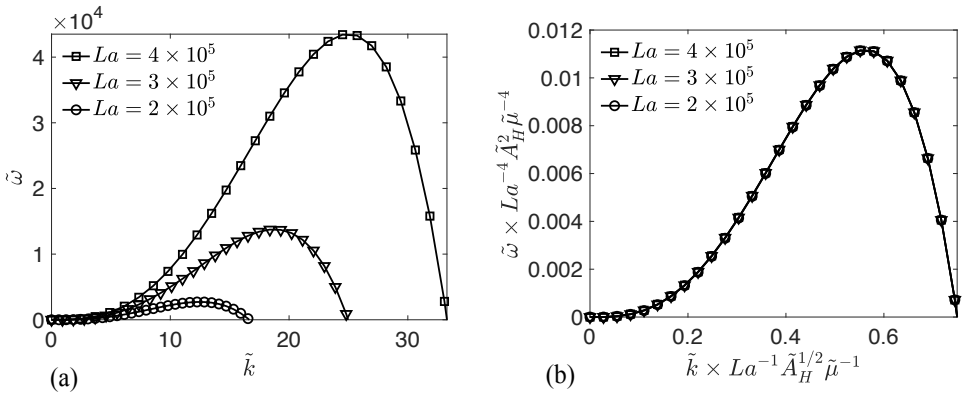

FIGURE 4. Dispersion relation, Eq. (4.8), for multiple values of La with $\tilde{A}_H = 3.354 \times 10^4$ and $\tilde{\mu} = 0.020$. The plot in (a) uses the scaling originally developed in Section 3.2, while the plot in (b) uses the new scalings of Section 4.3.

matches the earlier simplified limit, the solutions do not converge toward Eq. (3.13) as La is increased/decreased in contrast to the solutions of the potential-flow theory. Rather, the solution to Eq. (4.7) matches Eq. (3.13) only when $La \approx (1/2)\sqrt{\tilde{A}_H/\tilde{\mu}}$.

The second scenario takes place when $La > \sqrt{(2/3)}\tilde{A}_H^{1/2}\tilde{\mu}^{-1}$, where we see dispersion curves in the form of the plots shown in Figure 4(a). These plots belong to $La = 4 \times 10^5$, 3×10^5, and 2×10^5, corresponding to air films of thicknesses $h_0 = 1.82$ mm, 1.365 mm, and 0.91 mm surrounded by bulk water sections ($\tilde{A}_H = 3.354 \times 10^4$ and $\tilde{\mu} = 0.020$). From Figure 4(a), we observe that while La is only varied by a factor of two, the nondimensional unstable wave numbers and nondimensional growth rates vary significantly, indicating that the scaling laws for both of these quantities are different from all the regimes we have so far encountered. More precisely, the system is unstable for $\sqrt{3/8} < \tilde{k} < (3/4)\tilde{\mu}La\tilde{A}_H^{-1/2}$, corresponding to dimensional wavelengths of $8.378h_0(\mu_b/\mu_f) < \lambda < 10.26\sqrt{\sigma/A_H}h_0^2$. This range of unstable wavelengths is differ-

ent from the wavelength scaling that was predicted earlier by balancing surface-tension forces with van der Waals forces. Similarly, the nondimensional growth rate scales with $La^4\tilde{A}_H^{-2}\tilde{\mu}^4$, corresponding to the dimensional scaling of $\omega \sim (\mu_f^3\sigma)/(\mu_b^4 h_0)$, which is also different from earlier predictions of the growth-rate scaling. By utilizing these modified scalings, we see that the dispersion curves indeed collapse in Figure 4(b). It is worth noting that in this scenario, attractive van der Waals forces do not affect the instability, while larger film fluid viscosity and surface tension reduce the time scale of the instability (destabilize the system). On the other hand, increasing the bulk fluid viscosity or film thickness increases the time scale of instability (stabilizes the system). The underlying mechanism for this mode of instability is related to the interplay between capillary pressure and viscous pressure buildup in the bulk fluid due to shear from the flow inside the film. Further investigation of the nature of this instability is deferred to future work.

4.4. *Conditions for validity*

The analysis presented so far in Section 4 is valid only if lubrication theory holds in the film and Stokes flow holds in the bulk sections. In Section 4.3, we showed that two drastically different scenarios take place depending on the film thickness.

For thinner films, i.e., $La < \sqrt{(2/3)}\tilde{A}_H^{1/2}\tilde{\mu}^{-1}$, the wavelength and growth-rate scalings are similar to those of the potential-flow limit. First, the thin film approximation should hold. Second, the instability time scale should be much larger than the vorticity-diffusion time scale required for a shear layer to be sustained, which may be approximated as the time scale required for the surface velocity to be of the same order as the characteristic film velocity. The Stokes-flow limit is thus valid if

$$\tilde{A}_H^{1/2} \ll La, \quad \tilde{A}_H^{2/3}\tilde{\mu}^{-1/3} \ll La < \sqrt{(2/3)}\tilde{A}_H^{1/2}\tilde{\mu}^{-1}. \tag{4.9}$$

For thicker films where $La > \sqrt{(2/3)}\tilde{A}_H^{1/2}\tilde{\mu}^{-1}$, the wavelength of instabilities scales as $h_0\tilde{\mu}^{-1}$. Thus, lubrication theory holds as long as $\tilde{\mu} \ll 1$. In addition, we require that the instability time scale be much larger than the vorticity-diffusion time scale required for the surface and film velocities to be of the same order. This is equivalent to $La \ll \tilde{\mu}^{-3}$ based on the growth-rate scaling for these thick films. Put briefly, Eq. (4.8) is valid if

$$\tilde{\mu} \ll 1, \quad \sqrt{(2/3)}\tilde{A}_H^{1/2}\tilde{\mu}^{-1} < La \ll \tilde{\mu}^{-3}. \tag{4.10}$$

More generally, $\tilde{\mu} \ll \tilde{A}_H^{-1/4}$ and $\tilde{\mu} \ll 1$ are prerequisites for the existence of a range of film thicknesses in which Stokes flow in the bulk and lubrication theory in the film can be assumed in both scenarios, based on Eq. (4.9). Note that the Stokes-flow limit strictly does not hold when the instability first develops, as the viscous layer in the bulk has not yet had time to develop to a finite thickness at this point. A more rigorous analysis where the potential-flow limit is used to generate initial conditions for the Stokes-flow analysis is deferred to future work (see also Kaur & Leal 2009). This correction is expected to be minor as long as the aforementioned limits are satisfied.

5. Applications

For two different $\tilde{\mu}$ values, Figures 5 and 6 present regime diagrams in terms of the dimensionless numbers La and $\tilde{A}_H$, depicting where the potential-flow and Stokes-flow analyses (presented in Sections 3 and 4, respectively) are valid. The theory developed in this work enables access to a wider range of $(La, \tilde{A}_H)$ combinations for which a dispersion

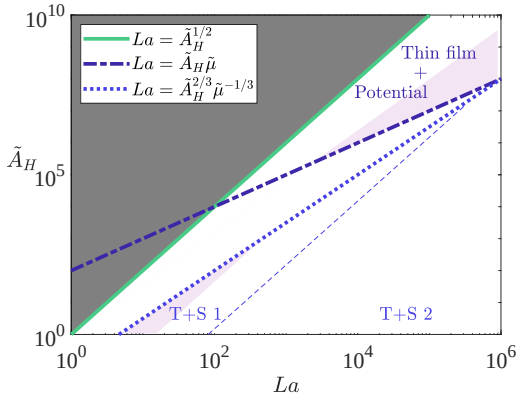

FIGURE 5. Regime diagram for $\tilde{\mu} = 10^{-2}$. The thin film approximation is not valid in the dark-shaded region. The bulk flow may be neglected in the light-shaded regions (purple in the online version of this brief). Note that the demarcations of regimes are only order-of-magnitude estimates. The dashed line demarcates the division between the two scenarios considered in the Stokes-flow limit. The first scenario, denoted T+S 1, corresponds to Eq. (4.9), while the second scenario, denoted T+S 2, corresponds to Eq. (4.10). In the unlabeled and unshaded region between the dash-dotted and dotted lines, the full Navier-Stokes equations must be considered in the bulk. This limit is not studied in this work.

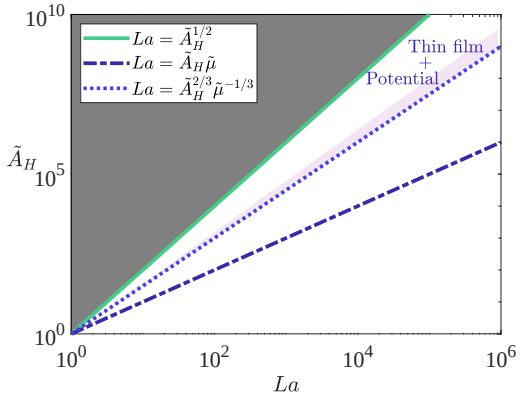

FIGURE 6. Regime diagram for $\tilde{\mu} = 10^{0}$. Note that the Stokes-flow limit is not valid anywhere in the regime diagram because $\tilde{\mu} = O(1)$. For a description of the shaded regions, as well as the unlabeled and unshaded regions, refer to the caption of Figure 5.

relation may be derived, especially in cases where the flow in the bulk fluid cannot be neglected. Note that the upper bound of the Stokes-flow analysis, i.e., $La \ll \tilde{\mu}^{-3}$, is outside the range of parameters considered in Figure 5. Note also that the Stokes-flow analysis is not valid at $\tilde{\mu} \gtrsim 1$, e.g., in Figure 6.

Table 1 lists the regimes of validity and characteristic film thicknesses for the potential-flow and Stokes-flow analyses in Sections 3 and 4, respectively, for different film–bulk fluid pairings. The potential-flow analysis is especially suited to gaseous films in molten metals, as well as superfluid films. For a given fluid pairing, or $\tilde{A}_H$ and $\tilde{\mu}$, the Stokes-flow analysis is valid at larger film thicknesses, or La, than the potential-flow analysis if the latter is valid, provided $\tilde{\mu} \ll \tilde{A}_H^{-1/4}$, $\tilde{\mu} \ll 1$, and the film remains significantly thinner than

Film	Bulk	$\tilde{\mu}$	$\tilde{A}_H^{1/2}$	Valid? (P)	h_0 (P)	Valid? (S)	h_0 (S)
Oil	Air	5.2×10^2	4×10^{-7}	No	N/A	No	N/A
Oil	Water	1.1×10^1	5×10^{-4}	No	N/A	No	N/A
Water	Air	4.7×10^1	9×10^{-5}	No	N/A	No	N/A
Air	Oil	1.9×10^{-3}	9×10^1	No	N/A	Yes	1 mm
Water	Oil	9.1×10^{-2}	5×10^{-2}	No	N/A	Yes	20 µm
Air	Water	2.1×10^{-2}	2×10^2	Limited	2 nm	Yes	400 nm
Air (1100 K)	Molten NaCl	4.4×10^{-2}	6×10^1	Limited	1 nm	Yes	80 nm
Air (1400 K)	Molten Cu	1.3×10^{-2}	2×10^3	Yes	10 nm	Yes	100 nm
H_2 (1800 K)	Molten Ag	8.7×10^{-3}	1×10^4	Yes	50 nm	Limited	80 nm

TABLE 1. Validity of potential-flow (P) and Stokes-flow (S) analyses for various film–bulk fluid pairings. The columns labeled h_0 denote characteristic film thicknesses within the regime of validity (if any) for each analysis. Limited means that the range of valid h_0 spans less than one order of magnitude. The properties of 10-cSt silicone oil are taken to be representative of oil. Unless otherwise stated, material properties at a temperature of 300 K are used. The Hamaker constants employed here are mostly order-of-magnitude estimates due to a paucity of data. Not included here is a superfluid ^{4}He film, which would have zero viscosity and almost certainly be entirely in the potential-flow regime if established in a suitable bulk. Note that since $\tilde{A}_H \ll 1$ and $\tilde{\mu} \gg 1$ in the first three fluid pairings, the potential-flow and Stokes-flow limits are respectively invalid. Since this simultaneously corresponds to a small density and a small dynamic viscosity in the bulk fluid, the conventional thin film analysis neglecting the bulk flow may be applied to these pairings if the thin film approximation $\tilde{A}_H^{1/2} \ll La$ is valid.

other externally imposed length scales. For example, the Stokes-flow analysis is nominally suitable for an air film in oil over a broad range of film thicknesses up to 1 mm as noted in Table 1, but the larger end of this range is typically also larger than externally imposed length scales. Notwithstanding this, the Stokes-flow analysis is generally suited to thin films of a variety of film–bulk fluid pairings at commonly encountered film thicknesses where the bulk is sufficiently more viscous than the film, including the coalescence of emulsions, splashing of molten salts, and breaking waves as highlighted in Section 1.

6. Conclusions

The linear stability of a thin fluid film sandwiched between two semi-infinite sections of a bulk fluid is examined in the limits where intermolecular van der Waals forces are important and motion in the bulk fluid cannot be neglected. The limiting regimes of potential flow and Stokes flow in the bulk fluid are examined. Dispersion relations are derived for both regimes, and a regime diagram is provided to specify when each limit holds for various film–bulk fluid pairings and film thicknesses.

The potential-flow analysis is shown to reduce to a conventional thin film dispersion relation when $\tilde{A}_H^{5/8} \ll La$, for which the bulk motion can be neglected. In addition, the potential-flow regime is shown to exist only when van der Waals forces are sufficiently strong, i.e., $\tilde{A}_H \gg 1$. Note also that stabilization by surfactants is beyond the scope of this work, both because surface-tension gradients and their effect on surface mobility are not considered, and because the thin film approximation $h_0 \ll \lambda_{cr}$ is more likely to be violated in this limit of low surface tension since $\lambda_{cr} \propto \sqrt{\sigma}$.

The limit of Stokes flow within the bulk sections is also examined. It is observed that depending on the film thickness, two scenarios can take place for the instability. While one scenario, which corresponds to thinner films, has length and time scales that match those of the potential-flow analysis and also conventional studies that neglect the bulk fluid, the other scenario, related to thicker films, results in growth rates that do not depend on intermolecular forces and happens at wavelengths that can no longer be explained by the balance between intermolecular and capillary forces. Rather, capillary-viscous interactions involving the film and bulk fluids are responsible for the second scenario. In both scenarios, the Stokes-flow regime only exists when the bulk dynamic viscosity is sufficiently large, i.e., $\tilde{\mu} \ll \tilde{A}_H^{-1/4}$ and $\tilde{\mu} \ll 1$.

A regime diagram is also provided to demarcate the regimes of validity of the two limiting analyses in terms of La, $\tilde{A}_H$, and $\tilde{\mu}$. The analysis in this work enables access to a broader range of $(La, \tilde{A}_H)$ combinations. In particular, flow in the bulk fluid cannot be neglected in certain subsets of both the potential-flow and the Stokes-flow regimes at small $\tilde{\mu}$, as well as in the potential-flow regime at large $\tilde{\mu}$. Note that the Stokes-flow limit is invalid when $O(\tilde{\mu}) \gtrsim 1$.

In summary, this work systematically generalizes the linear stability of thin fluid films to a variety of bulk flow regimes and provides a dispersion relation for each of these limits, including a reference diagram to determine when each limit holds. This enables thin film stability theory to be extended to the analysis of antibubbles, splashing ionic liquids in carbon-capture infrastructure and melt pools in advanced manufacturing processes, as well as emulsion stability, among other flows of practical importance.

Acknowledgments

The authors are grateful to Javier Urzay, Ali Mani, and Parviz Moin for early discussions on this topic. The authors also thank Tim Flint for helpful comments on an early draft of this manuscript. This work was supported by the Office of Naval Research (ONR) under grants #N00014-15-1-2523 and #N00014-15-1-2726. W. H. R. Chan was funded by a National Science Scholarship from the Agency for Science, Technology and Research in Singapore, and by a Franklin P. and Caroline M. Johnson Fellowship from Stanford University.

REFERENCES

Baldessari, F., Homsy, G. & Leal, L. G. 2007 Linear stability of a draining film squeezed between two approaching droplets. *J. Colloid Interf. Sci.* **307**, 188–202.

Couder, Y., Fort, E., Gautier, C.-H. & Boudaoud, A. 2005 From bouncing to floating: noncoalescence of drops on a fluid bath. *Phys. Rev. Lett.* **94**, 177801.

Craster, R. V. & Matar, O. K. 2009 Dynamics and stability of thin liquid films. *Rev. Mod. Phys.* **81**, 1131–1198.

Dorbolo, S., Reyssat, E., Vandewalle, N. & Quéré, D. 2005 Aging of an antibubble. *Europhys. Lett.* **69**, 966.

Erneux, T. & Davis, S. H. 1993 Nonlinear rupture of free films. *Phys. Fluids* **5**, 1117–1122.

González, A. G., Diez, J. A. & Sellier, M. 2016 Inertial and dimensional effects on the instability of a thin film. *J. Fluid Mech.* **787**, 449–473.

Ida, M. P. & Miksis, M. J. 1996 Thin film rupture. *Appl. Math. Lett.* **9**, 35–40.

Ivanov, I. B., Radoev, B., Manev, E. & Sheludko, A. 1970 Theory of the critical thickness of rupture of thin liquid films. *T. Faraday Soc.* **66**, 1262–1273.

Kaur, S. & Leal, L. G. 2009 Three-dimensional stability of a thin film between two approaching drops. *Phys. Fluids* **21**, 072101.

Kirkinis, E. & Davis, S. H. 2015 Stabilization mechanisms in the evolution of thin liquid-films. *P. Roy. Soc. A-Math. Phy.* **471**, 20150651.

Moreno-Boza, D., Martínez-Calvo, A. & Sevilla, A. 2020*a* The role of inertia in the rupture of ultrathin liquid films. *Phys. Fluids* **32**, 112114.

Moreno-Boza, D., Martínez-Calvo, A. & Sevilla, A. 2020*b* Stokes theory of thin-film rupture. *Phys. Rev. Fluids* **5**, 014002.

Oron, A., Davis, S. H. & Bankoff, S. G. 1997 Long-scale evolution of thin liquid films. *Rev. Mod. Phys.* **69**, 931.

Prévost, M. & Gallez, D. 1986 Nonlinear rupture of thin free liquid films. *J. Chem. Phys.* **84**, 4043–4048.

Ruckenstein, E. & Jain, R. K. 1974 Spontaneous rupture of thin liquid films. *J. Chem. Soc. Farad. T. 2* **70**, 132–147.

Sharma, A. & Ruckenstein, E. 1986*a* An analytical nonlinear theory of thin film rupture and its application to wetting films. *J. Colloid Interf. Sci.* **113**, 456–479.

Sharma, A. & Ruckenstein, E. 1986*b* Finite-amplitude instability of thin free and wetting films: prediction of lifetimes. *Langmuir* **2**, 480–494.

Sheludko, A. 1967 Thin liquid films. *Adv. Colloid Interfac.* **1**, 391–464.

Thoroddsen, S. T., Thoraval, M. J., Takehara, K. & Etoh, T. 2012 Micro-bubble morphologies following drop impacts onto a pool surface. *J. Fluid Mech.* **708**, 469.

Vaynblat, D., Lister, J. R. & Witelski, T. P. 2001 Rupture of thin viscous films by van der Waals forces: evolution and self-similarity. *Phys. Fluids* **13**, 1130–1140.

Vrij, A. 1966 Possible mechanism for the spontaneous rupture of thin, free liquid films. *Discuss. Faraday Soc.* **42**, 23–33.

Vrij, A. & Overbeek, J. T. G. 1968 Rupture of thin liquid films due to spontaneous fluctuations in thickness. *J. Am. Chem. Soc.* **90**, 3074–3078.

Williams, M. B. & Davis, S. H. 1982 Nonlinear theory of film rupture. *J. Colloid Interf. Sci.* **90**, 220–228.

Yiantsios, S. G. & Higgins, B. G. 1991 Rupture of thin films: nonlinear stability analysis. *J. Colloid Interf. Sci.* **147**, 341–350.

Zhang, W. W. & Lister, J. R. 1999 Similarity solutions for van der Waals rupture of a thin film on a solid substrate. *Phys. Fluids* **11**, 2454–2462.

Zhao, T. Y. & Patankar, N. A. 2020 The thermo-wetting instability driving Leidenfrost film collapse. *Proc. Natl. Acad. Sci. USA* **117**, 13321–13328.